INTERNATIONAL JOURNAL OF INTEGRATED ENGINEERING
ISSN: 2229-838X e-ISSN: 2600-7916

IJIE

Vol. 16 No. 5 (2024) 34-45
https://publisher.uthm.edu.my/ojs/index.php/ijie

Numerical Analysis on the Aerodynamic Performance of a High-speed Train Operating on Various Embankment Heights Under the Influence of Crosswinds

Nik Nur Amyra Adilla Noor Khairullah[1], Izuan Amin Ishak[1]*, Mohammad Arafat[1], Nurshafinaz Mohd Maruai[2], Fadhilah Mohd Sakri[3], Amir Khalid[4]

[1] *Department of Mechanical Engineering Technology, Faculty of Engineering Technology, Universiti Tun Hussein Onn Malaysia (UTHM), 84600 Pagoh, Johor, MALAYSIA*

[2] *Department of Mechanical Precision Engineering, Malaysia-Japan International Institute of Technology (MJIIT), Universiti Teknologi Malaysia (UTM), Jalan Sultan Yahya Petra, 54100, Kuala Lumpur, MALAYSIA*

[3] *Aerospace Section, Universiti Kuala Lumpur Malaysian Institute of Aviation Technology (UniKL MIAT), Lot 2891, Jalan Jenderam Hulu, Kampung Jenderam Hulu, 43900 Dengkil, Selangor, MALAYSIA*

[4] *Faculty of Mechanical and Manufacturing Engineering, Universiti Tun Hussein Onn Malaysia (UTHM), Persiaran Tun Dr. Ismail, 86400 Parit Raja, Johor, MALAYSIA*

*Corresponding Author: izuan@uthm.edu.my

DOI: https://doi.org/10.30880/ijie.2024.16.05.004

Article Info

Received: 24 November 2023
Accepted: 5 May 2024
Available online: 1 August 2024

Keywords

Train safety, crosswind angle, embankment height, aerodynamic characteristics, Next Generation High-speed Train (NG-HST), computational fluid dynamics (CFD), reynolds number

Abstract

Given the unavoidable geographical surface, railings must be raised above ground level in some cases, which is known as an embankment. It was discovered that the height of the embankment had a significant influence on the slipstream on the train's leeward side especially during crosswind conditions. The primary objectives of this study were to investigate the impact of varying embankment heights on the aerodynamic characteristics of a high-speed train under different crosswind conditions using computational fluid dynamics (CFD) analysis. The German Aerospace Center DLR's Next-Generation High-speed Train (NG-HST) model has been used for this study. The yaw angles (ψ) are ranging from 10° to 50° in 10° increments. The Reynolds number based on the model's height and freestream velocity at the computational domain is 1.3×10^6. In the results, it shows that embankment height and crosswind ψ has a significant impact on the aerodynamic characteristics. Essential aerodynamic parameters that have a significant impact on train stability, such as the drag, lift, and side force coefficients, as well as the roll, yaw, and pitch moment coefficients, revealed that the higher the ψ, which included 40° and 50°, produced poor results compared to the lower ψ, which included 10°, 20°, and 30°. In terms of visual appearance, rising of crosswind angles have a greater impact on the formation of vortices on the leeward side of the train body and embankment. Thus, it can be concluded that the embankment heights and crosswind angles are crucial in determining train safety operations.

1. Introduction

Crosswind, as one of the primary sources of train lateral force, poses a threat to train overturning stability. Crosswind stability of rail vehicles has been a focus of research for several decades, primarily due to vehicle overturning accidents and increased speeds. During operation, trains are frequently exposed to crosswinds, which affects their aerodynamic performance [1].

When a train travels in windy conditions, it encounters a crosswind. When the wind and train velocity combine, they create a relative wind that loads the train [2]. Aerodynamic loads on railway vehicles exposed to strong crosswinds can have a significant impact on operational safety. This is due to the fact that they can alter vehicle operational stability by increasing the risk of overturning. Crosswind effects become especially important at high operating speeds [3], [4]. Overturning a high-speed train travelling at 300 km/h would be fatal. The strength of aerodynamic loads increases as the relative velocity between the side wind and train increases [5].

Due to the general unavoidable geographical surface, the railings must be raised above the ground in some cases. Because the railway level rises at higher altitudes, the vehicle's aerodynamic stability suffers. High embankments contribute significantly to the accumulated risk of mechanical safety violations [6]. Aerodynamic forces increase significantly for trains running on infrastructure, potentially increasing the likelihood of trains derailing and overturning [6], [7]. Strong winds will be prevented by the embankment in windy areas, resulting in an accelerating effect on the embankment [7].

There have only been a few numerical studies on the aerodynamics of trains travelling over infrastructure. As a result, the amount of data available for this study's reference is quite limited. Diedrichs et al., focused solely on the effect of an embankment with a fixed height and slope in their study [8]. When compared to the level ground condition, the 6-meter-high embankment reduced the allowed crosswind speed by about 20%, according to their research. According to Zhou et al., the maximum side force for a rail vehicle travelling on an embankment increases at $\psi = 50°$, and the overturning moment coefficient follows a similar pattern [9]. Further to that, according to Ishak et al., the crosswind yaw angle and the ground condition in which the train is travelling have a significant impact on the aerodynamic loads [10]. When comparing the bridge cases to the baseline scenario, i.e., the flat ground case, important parameters that have a significant impact on train stability, such as coefficient of side force (C_s), rolling moment (C_{rl}), lift force (C_l), and drag force (C_d), revealed that the bridge cases produced the worst results of these parameters (FGC).

Therefore, numerical simulations using computational fluid dynamics are used to investigate the impact of varying embankment heights on the aerodynamic characteristics and flow structure of a high-speed train under different crosswind conditions. The crosswind angles (ψ) range from 10° to 50° with 10° increments, and the embankment heights are set to 1 m, 1.5 m, 2.5 m, and 4 m.

2. Methods

2.1 Research Framework

Current research work was carried out using CFD analysis. The geometry modelling of the NG-HST and embankment structure was performed on Solidworks software. Following the completion of geometry modelling, meshing and computational domain for simulation is generated in ANSYS Fluent software. The validation process then begins with a grid independence test and comparison of simulation results with reference paper. The final case simulations were run with different embankment heights and crosswind conditions. The normal embankment height for high-speed trains is a critical factor that influences various aspects of railway operations and typically ranges from 1 to 6 m [11], [12] In the current study, embankment heights ranging from 1 to 4 m were considered, as illustrated in Fig.1. On the other hand, a total of five crosswind yaw angles are tested for each case: 10°, 20°, 30°, 40°, and 50°. The analysis concentrated on the aerodynamic loads and flow structure around the train on various embankment heights and crosswind conditions.

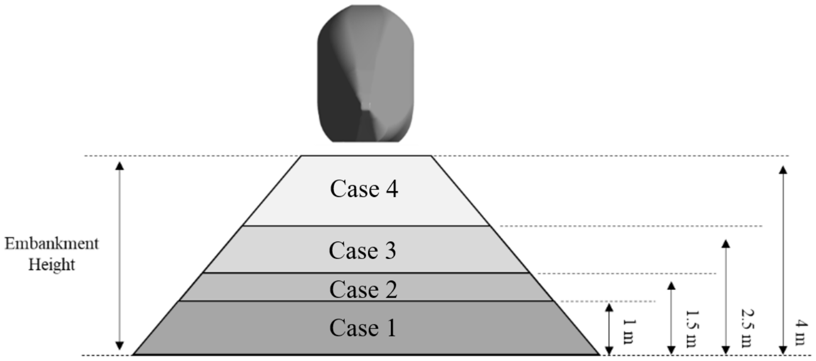

Fig.1 *The train model with various embankment height*

2.2 NG-HST Model

The model used in this study is a simplified version of Next-Generation High-Speed Train (NG-HST) which originally developed by German aerospace center (DLR) [13]. Fig. 2 shows a simplified model design created with Solidworks software. The train utilized is a 1/25th scaled model of the original size [14]. This is due to minimize computational cost followed by previous studies [15], [16].

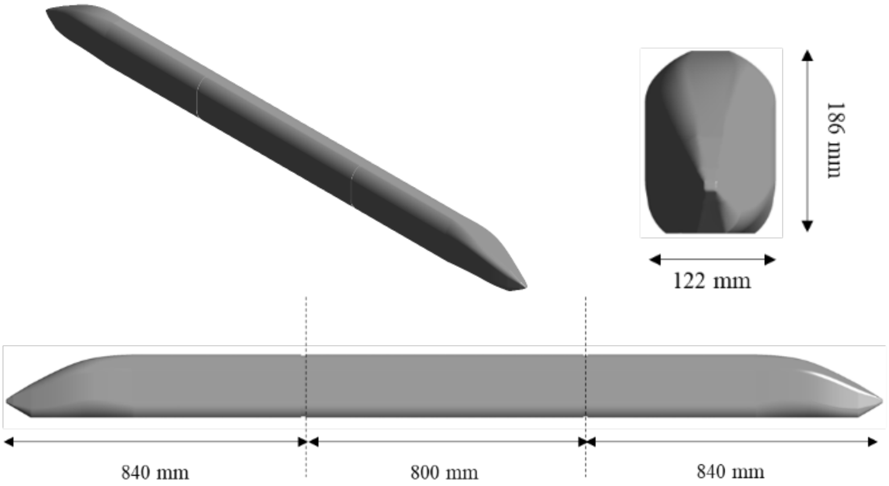

Fig. 2 *A high-speed train model used in the study*

2.3 Enclosure and Boundary Condition

A wider enclosure is constructed to provide a better mesh and more accurate findings. The fluid domain or enclosure is used by analytical tools to mimic fluid. Fig. 3 shows the train model with an embankment inside the enclosure, as well as the enclosure's isometric and front view dimensions.

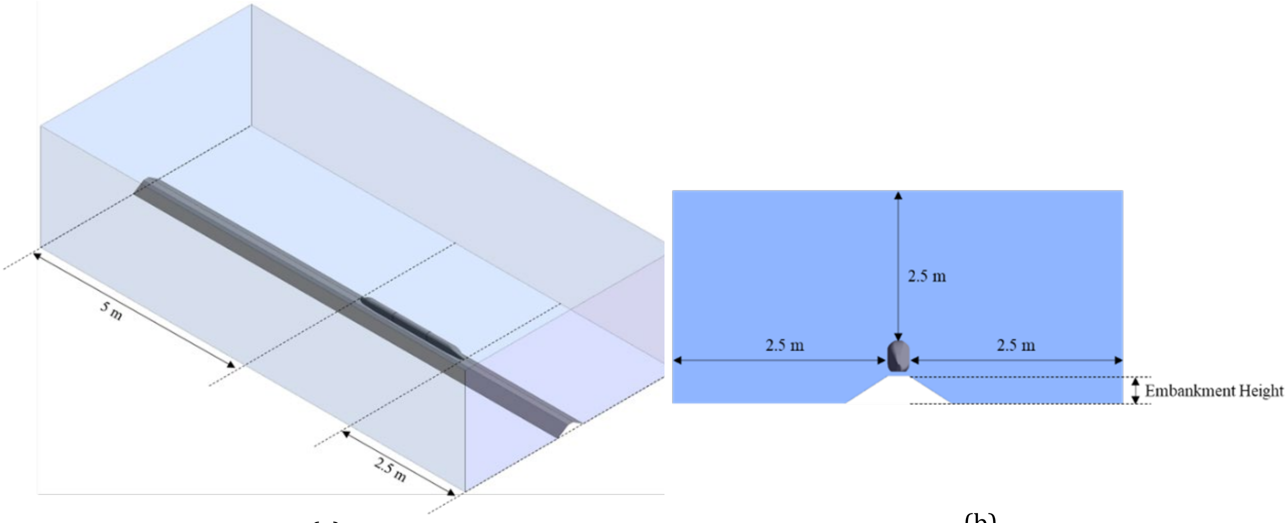

(a) (b)

Fig. 3 *The enclosure (a) The train model with an embankment inside the enclosure; (b) The enclosure's dimensions in isometric and front view*

Following the creation of the enclosure and Boolean, the model's boundary conditions, such as velocity inlet, pressure outlet, vehicle surface, and symmetry sides, should be established as shown in Fig. 4 and Table 1. Velocity at the inlet for the validation case was 60.25 m/s, reflecting a train speed of approximately 216 km/h. This choice allows for a direct comparison of the validation results with those from a previous study [17], [18]. However, for the final case simulations, a relative wind velocity of 111.11 m/s was used, corresponding to a specific crosswind angle. This is a requirement that must be met at all or part of the boundaries of a region where a series of differential conditions must be solved. Setting the boundary condition is critical for obtaining accurate results from the CFD study.

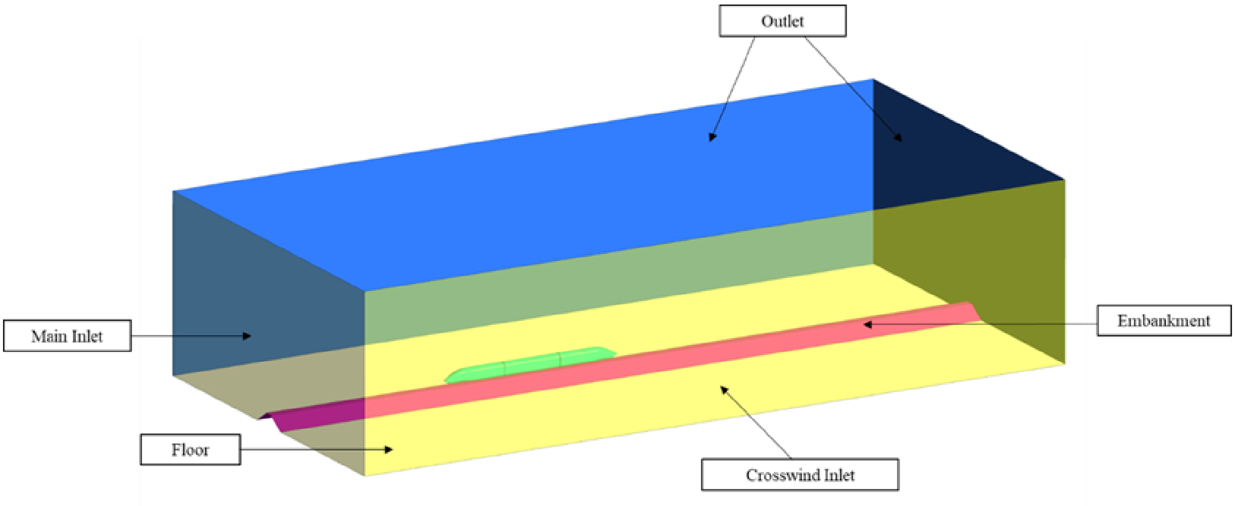

Fig. 4 *Boundary conditions for current numerical simulation*

Table 1 *Details and values of boundary condition*

Detail	Boundary Condition	Value
Inlet	Velocity Inlet	60.25 m/s
Outlet	Pressure Outlet	0 Pa (gauge)
Train Body	Wall Boundary	No Slip
Symmetry	Wall Boundary	Stationary
Reference	Temperature	298 K
Inlet	Velocity Inlet	60.25 m/s

2.4 Numerical Method and Solver Setting

When a train is traveling at high speeds, the flow around it can be accurately modeled as a three-dimensional incompressible flow process. For numerical simulations, an accurate turbulent transport equation is required. The Reynolds-averaged Navier-Stokes (RANS) simulation has been widely adopted as a numerical method for turbulent flow calculations, given its relatively high accuracy in predicting mean flow features and its more manageable computational demands [19]. In this study, RANS based on the standard k-ε turbulence model was employed due to its effectiveness in capturing turbulent behavior in vehicle aerodynamics [8], [20]. Additionally, 1000 iterations were computed to meet convergence criteria. The SIMPLE algorithm for pressure-velocity coupling was utilized, and a second-order scheme was chosen for the discretization of all variables.

2.5 Grid Independence Test

To obtain accurate results, an optimal grid design is required [21]. The grid independence test is commonly used to create an optimal grid. Based on the evaluation of various grid conditions, the grid independence test is a process used to find the optimal grid condition with the fewest number of grids while generating no difference in numerical results [22]. The ANSYS Meshing module was employed to generate meshes for five different resolutions, denoted as Mesh 1 to Mesh 5. Each mesh resolution was based on variations in surface size on the train, overall element sizes, and refinement zones. A polyhedral mesh type was used for the meshing. This type of meshing is particularly advantageous in capturing the details of irregular and curved surfaces, resulting in more accurate simulations. Mesh metrics, including an orthogonal quality greater than 0.63 and skewness less than 0.28, were maintained.

The CFD results from the ANSYS software for the validation study are compared using the coefficient of drag, C_d, obtained from the simulation. Fig. 5 depicts the comparison graph of the results of the coefficient of drag, C_d, for the five grid validation studies and the previous study by Fragner *et al.*[23]. The graph displays the number of elements for each of the mesh resolutions.

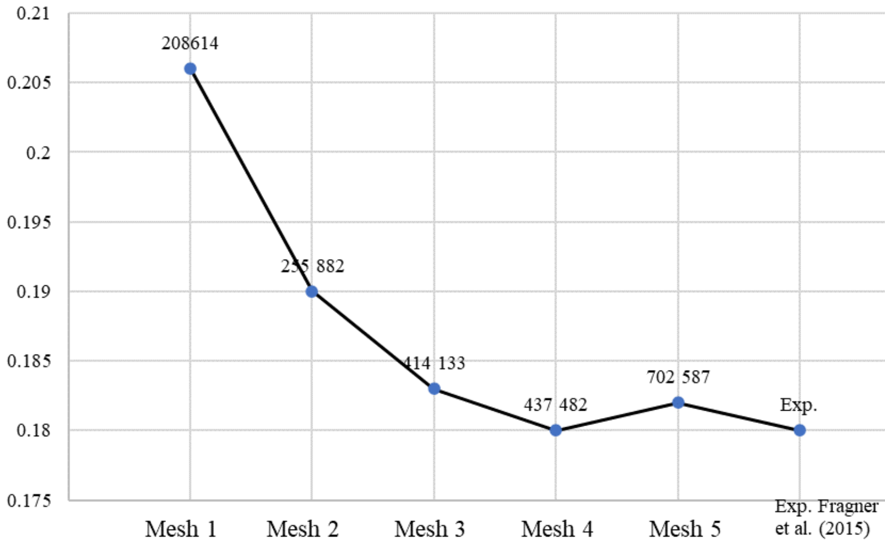

Fig. 5 *Comparison of* C_d *value from the five mesh cases and previous exp*

3. Results and Discussion

The numerical simulation results for a train moving on various embankment heights are discussed and analyzed in two main sections in which the flow structure results include streamline and vortex formations due to the changes in pressure acting on the train body and the aerodynamic loads results include the coefficient of aerodynamic forces like drag, side, and lift as well as moments like pitch, yaw and roll on the train body.

3.1 Flow Structure

Two different locations have been chosen to show the streamlines and pressure contour, as shown in Fig. 6. Plane 1 cuts through the middle of the train, while Plane 2 cuts through the rear of the train. These planes are essential to show how the pressure varies around the train body's various parts, as well as how flow separation and vortex forms.

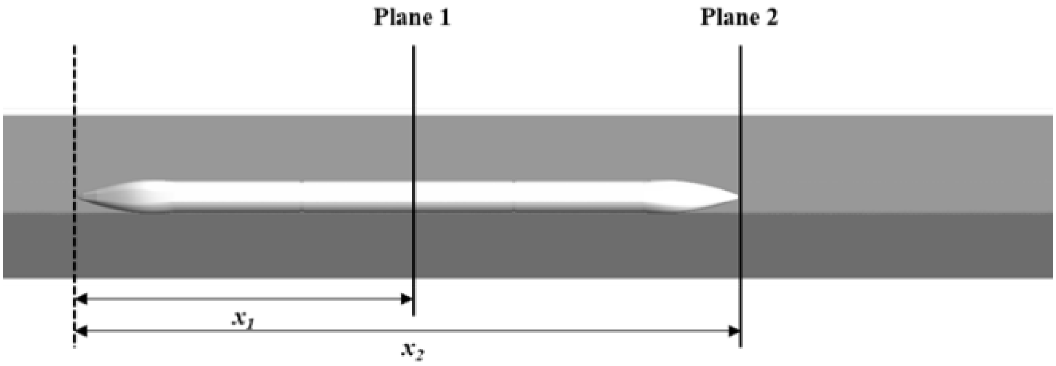

Fig. 6 *The plane's position used to visualize streamlines and pressure contours front top view. Plane 1:* $x_1 = 6.67H$ *and Plane 2:* $x_2 = 13.33H$

3.1.1 Streamlines at Different Locations

Fig. 7 shows the streamlines superimposed with pressure contour for different embankment heights and yaw angles at Plane 1. At the yaw angle (Ψ) of 10°, as the embankment height increases, the vortices on the leeward side of the train become visible. Case 1 shows a small region of negative pressure on the train's roof while cases 2, 3, and 4 show a gradual increase in negative pressure on the leeward side and on the train's roof.

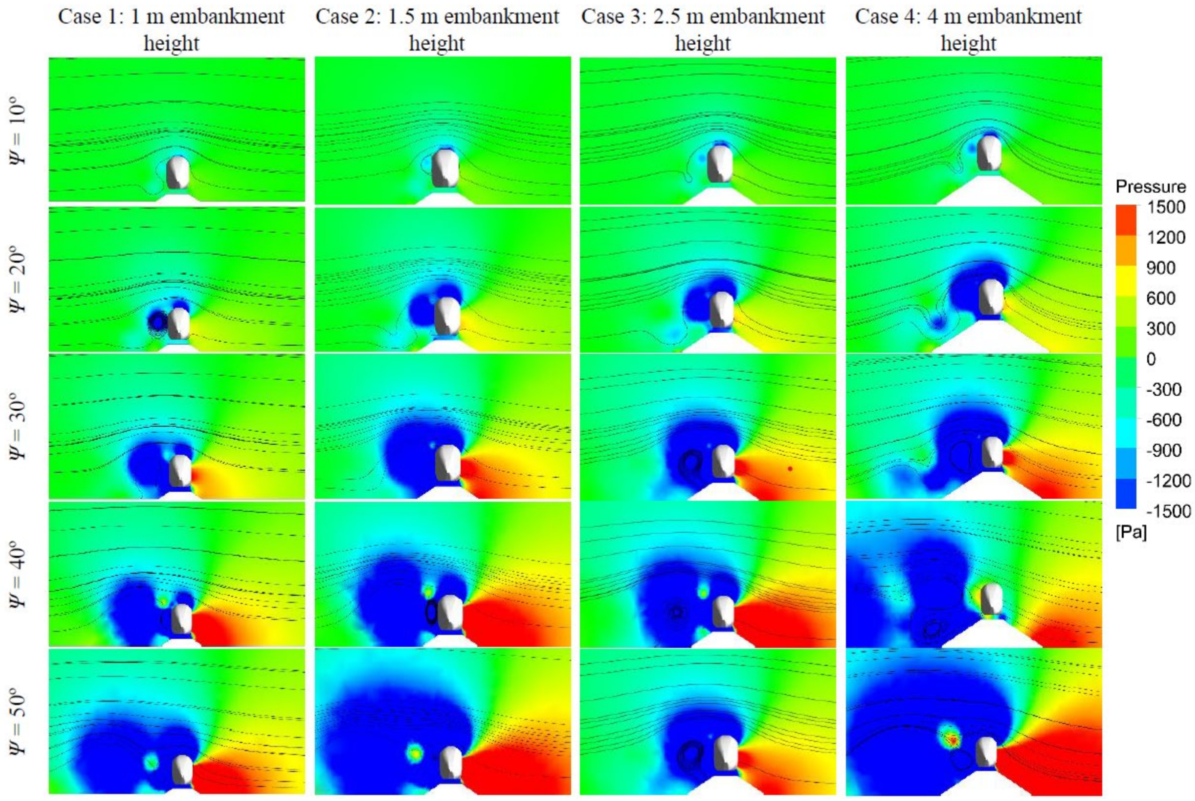

Fig. 7 *Streamlines superimposed with pressure contour for different embankment heights and yaw angles at Plane 1*

At Ψ = 20°, the vortices that form on the train's leeward side and roof are becoming more complex. The pattern is nearly similar to that seen at Ψ = 10°, but the negative pressure on the leeward side and on the train's roof becomes visible as the embankment height increases. The maximum negative pressure is seen in Case 4. Whereas the positive pressure that appears on the train's windward side is becoming more intense and nearly identical in all four cases.

At Ψ = 30°, the vortices that form on the leeward side, on the roof, and between the train's floor and the embankment are becoming more visible and complex. Negative pressure becomes dominant on the train's leeward side, on the roof, and between the train's floor and the embankment. At this crosswind angle, the positive pressure increases as the height of the embankments rise. This is because as the embankment height rises, it prevents the crosswind from passing through the train, putting pressure on the train's surface and the embankment on the windward side.

The pattern is nearly identical at higher yaw angles, which are 40° and 50°, as the vortices become more intense, complex, and unsteady. In Case 1, at Ψ = 50°, two groups of streamlines separated and formed two major vortices on the train's leeward side. Case 4 at the same yaw angle, on the other hand, has one flow separation that creates a major vortex on the train's leeward side due to wind loads on the train surface and the embankment. On the train's leeward side, on the roof, and between the train's floor and the embankment, negative pressure becomes dominant and more intense. However, at Ψ = 50°, cases 2 and 4, a tornado-like wind-shape forms with positive and nearly normal pressure in the center and negative pressure surrounding it. Positive pressure increases as the embankment's height increases.

In brief overview, this proves how increasing crosswind angles and embankment height affect vortex formation on the leeward side of the train body. When a crosswind from the train's windward side reaches the train surface, pressure rises, which increases as the yaw angle and embankment height rise.

Fig. 8 depicts streamlines superimposed on pressure contours at Plane 2 for different embankment heights and yaw angles. From the figure, the formation of vortices is unclear at Ψ = 10° in all four cases. There is a less visible negative pressure region, but there is an observable positive pressure region surrounding the train's surface. At Ψ = 20°, it can be seen that the vortices gradually form from one to two visible vortices from Case 1 to Case 4. The negative pressure can be seen on the train's leeward side, one near the train's surface and the other further away. Positive pressure has also been spotted on the train's upper edge and between the train's floor and the embankment.

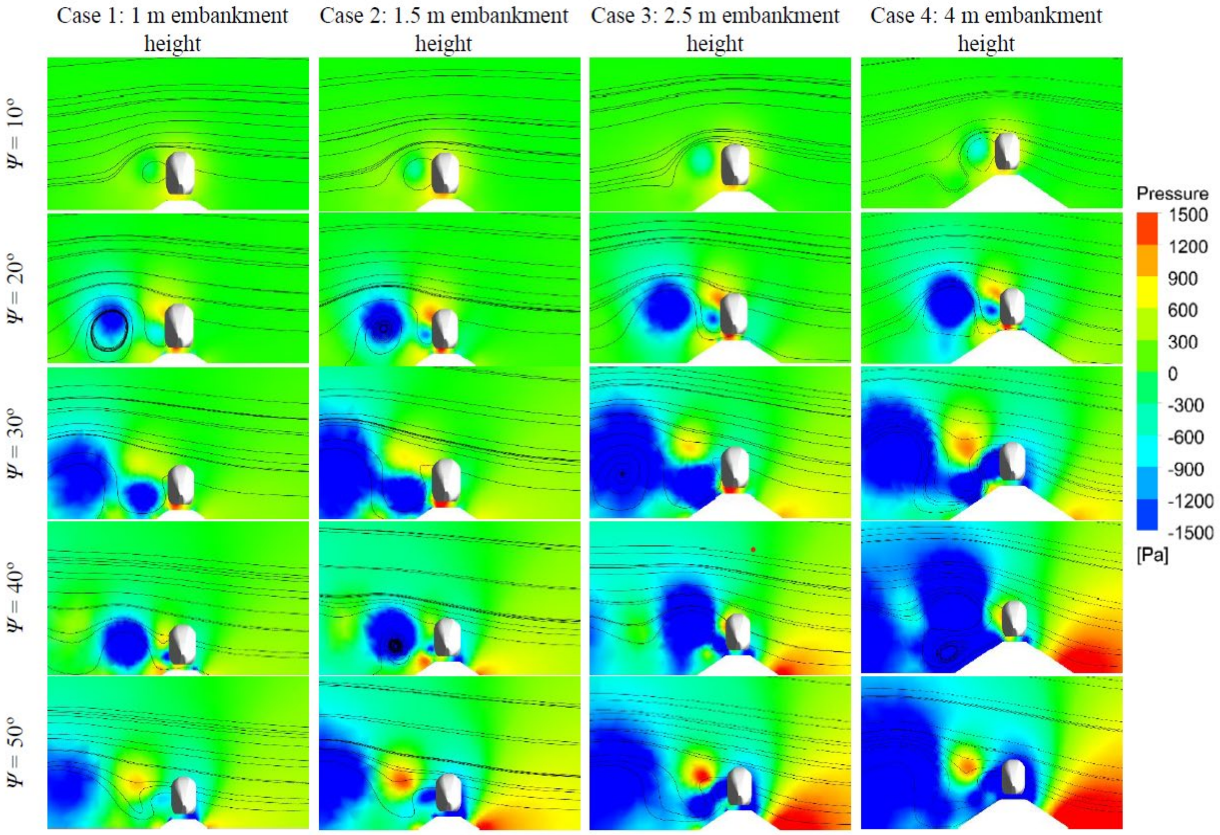

Fig. 8 *Streamlines superimposed with pressure contour for different embankment heights and yaw angles at Plane 2*

The vortices that form on the leeward side are becoming intense and complex at Ψ = 30°. On the train's leeward side, negative pressure takes over. Moreover, in Case 4, there is some negative pressure on the train's windward side. However, only cases 1, 2, and 3 show positive pressure between the train's floor and the embankment. The formation of vortices becomes more complex and intense at higher yaw angles, which are 40° and 50°, however, some of the vortices can be seen further away from the train's surface. On the leeward side, the negative pressure region takes over. In contrast to the result shown in Fig. 8, positive pressure on the windward side is not prominent at Plane 1. As the embankment height increased, so did the positive pressure on the windward side.

Based on the pressure contour, comparing both Plane 1 and Plane 2, the front of the train is ultimately more critical than the end of the train. It is noticeable that the low-pressure region forms due to the formation of vortices adhering to the train surface more at Plane 1 whilst it seems to be dispersed away as it leaves the body of the train as shown in Plane 2. Pressure differences between the windward area and the leeward area of the train become more critical as the yaw angle increases and as the embankment height increases. The aerodynamic loads, which likely determine whether or not the train is functioning safely, are influenced by the flow structure surrounding it, therefore, the higher the embankment, making it more hazardous in terms of safety.

3.1.2 Three-dimensional Flow Behavior

The pattern is nearly identical in all four cases; the higher the embankment height and yaw angle, the larger, more complex, and intense the vortices become, and they move further away from the train's surface. The vortex clearly began to form at the upper edge of the train. At Ψ = 10°, a vortex is formed and is less visible than one at Ψ = 20°. From Ψ = 30° to Ψ = 50°, the intensity of the vortex formation increases. The vortices form become more intense, larger, twisted, and moved further away from the train's surface. However, the vortices that form on the frontal leeward area vary depending on the flow direction, which is determined by the yaw angle conditions, and the height of the embankment for each case. For comparison, Fig. 9 (b) and (d), show differences in the shape of the vortices despite appearing identical. Fig. 9 (d), for example, has more intense and complex vortices that moved further away from the train's surface than the vortices formed in Fig. 9 (b).

Furthermore, based on the velocity contour color, it is clear that as the yaw angle increases, the positive velocity is maximum on the windward side of the train body, owing to the direct hit of wind load on the train's surface. As the yaw angle and embankment height increase, the high-velocity region becomes more visible on the train's frontal area and body. This is because the crosswind is prevented from passing through the train, causing the velocity contour on the train's body on the windward side to be at its maximum.

In general, the intensity of vortex formation decreases towards the train's rear. As the yaw angle and embankment height increase, it becomes pronounced in the frontal area and the body of the train. As a result, this demonstrates that, in comparison to other regions, the frontal part of the train is most affected by the aerodynamic loads caused by crosswinds.

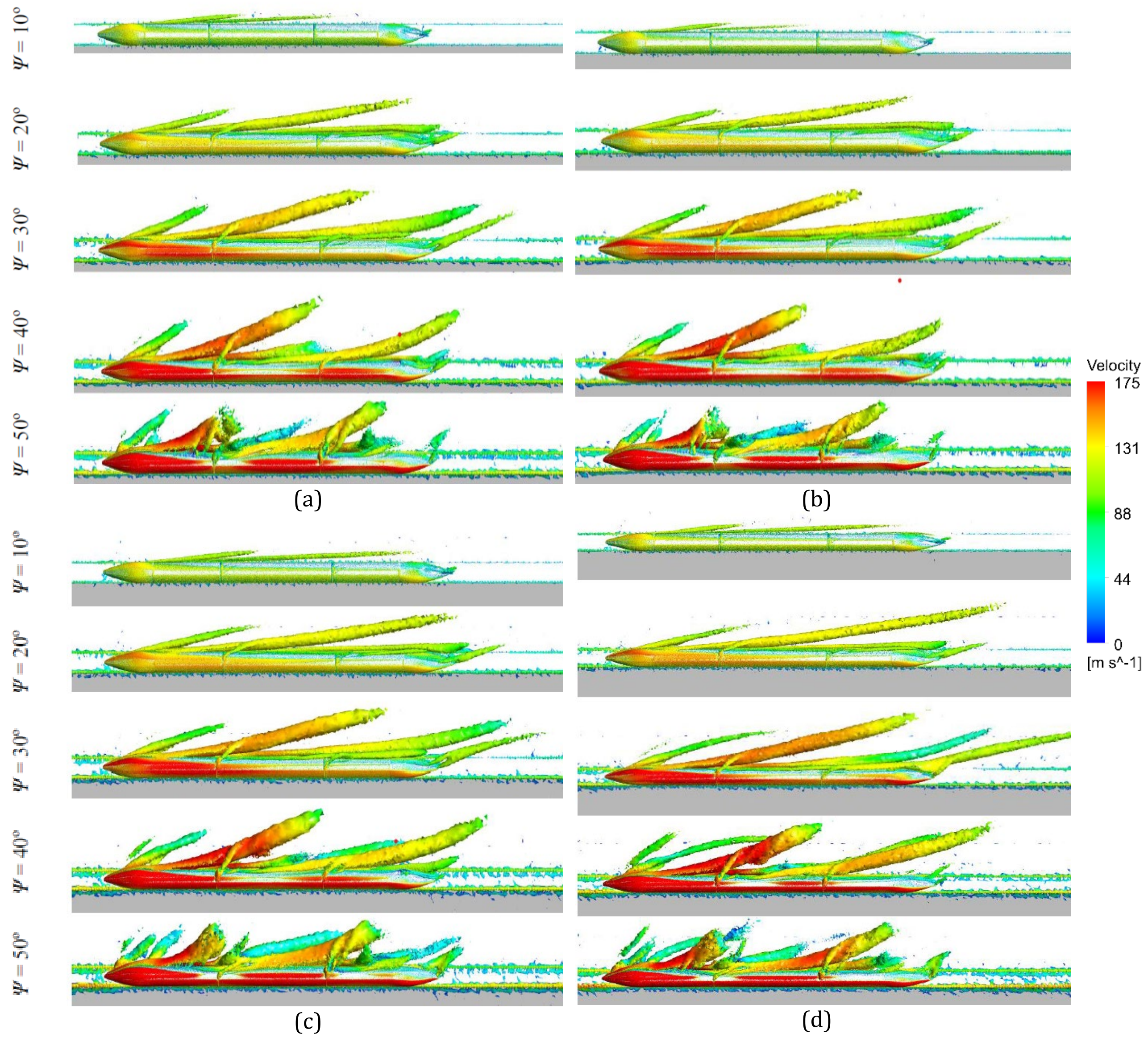

Fig.9 *Top view of vortices formation: (a) Case 1: 1 m embankment height; (b) Case 2: 1.5 m embankment height; (c) Case 3: 2.5 m embankment height; (d) Case 4: 4 m embankment height*

3.2 Aerodynamic Force and Moment Coefficients

Fig. 10 (a)-(c) shows the aerodynamic forces of the train for various embankment heights and yaw angles. In Fig. 10 (a), from Ψ = 0° to Ψ = 10°, the value of the drag force coefficient (C_d) is the same in all four cases. However, it starts to deviate as the crosswind increases as it is majorly affected by the rise in embankment heights. It is noticeable that a fluctuation in the drag force coefficient (C_d) emerges at Ψ = 30° to 50°. A decline in the drag force coefficient value can be seen at Ψ = 30°. This phenomenon occurs when the embankment height is 4 m, reflecting Case 4 as the most critical for aerodynamic performance. On the other side, it is notable that the embankment heights have little effect on the side force coefficient (C_s) as the pattern is nearly the same. From the graph, it can be seen that as the yaw angle increases, so does the C_s value due to the contact area of the train and wind loads on the windward side. Fig. 10 (c) depicts the train's lift force coefficients (C_l). As the yaw angle and embankment height increased, the C_l value gradually increased. At $\Psi = 30°$, the C_l value for Case 4 is slightly higher than the other cases; however, the C_l values for Cases 1–3 are roughly equivalent because the line pattern is remarkably similar.

Next, Fig. 11 (a) displays the train's rolling moment coefficients (C_{rm}) for various crosswind yaw angles and embankment heights. With rising embankment heights and yaw angles, the C_{rm} rises as well. From $\Psi = 0°$ to $\Psi = 30°$, the C_{rm} value gradually increases in all four cases. However, Case 4 continues to increase intensively in comparison to the other cases. The train's yawing moment coefficients (C_{ym}) for various embankment heights and yaw angles are shown in Fig. 11 (b). The C_{ym} value reduces to the negative moment region as the yaw angles increase. Lastly, the train's pitching moment coefficients (C_{pm}) are shown in Fig. 11 (c). From the graph, it can be seen that the C_{pm} value grows as the yaw angle does.

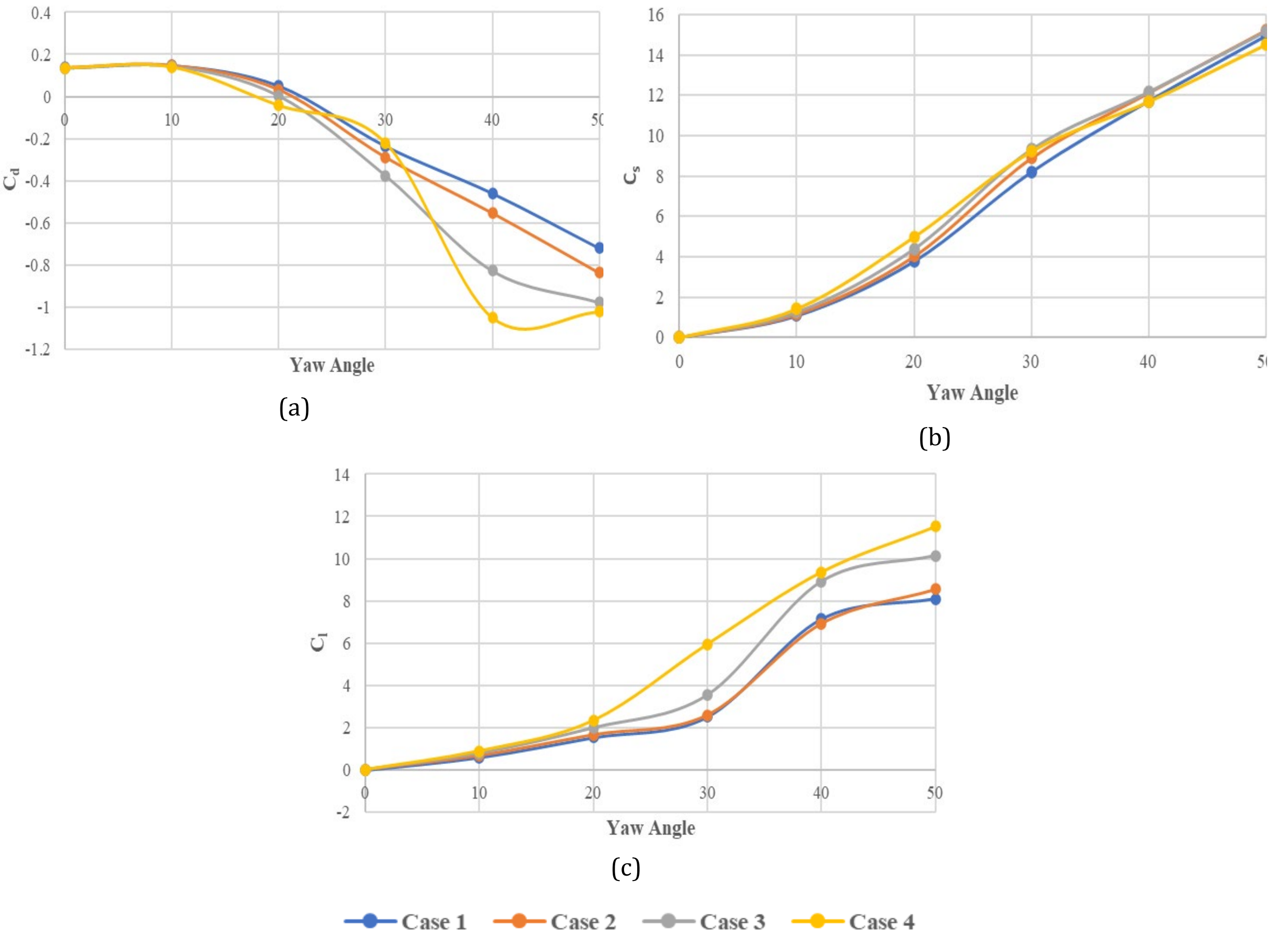

(a)

(b)

(c)

Fig. 10 *Time-averaged aerodynamic force and moment coefficients: (a) Drag force (C_d); (b) Side force (C_s); (c) Lift force (C_l)*

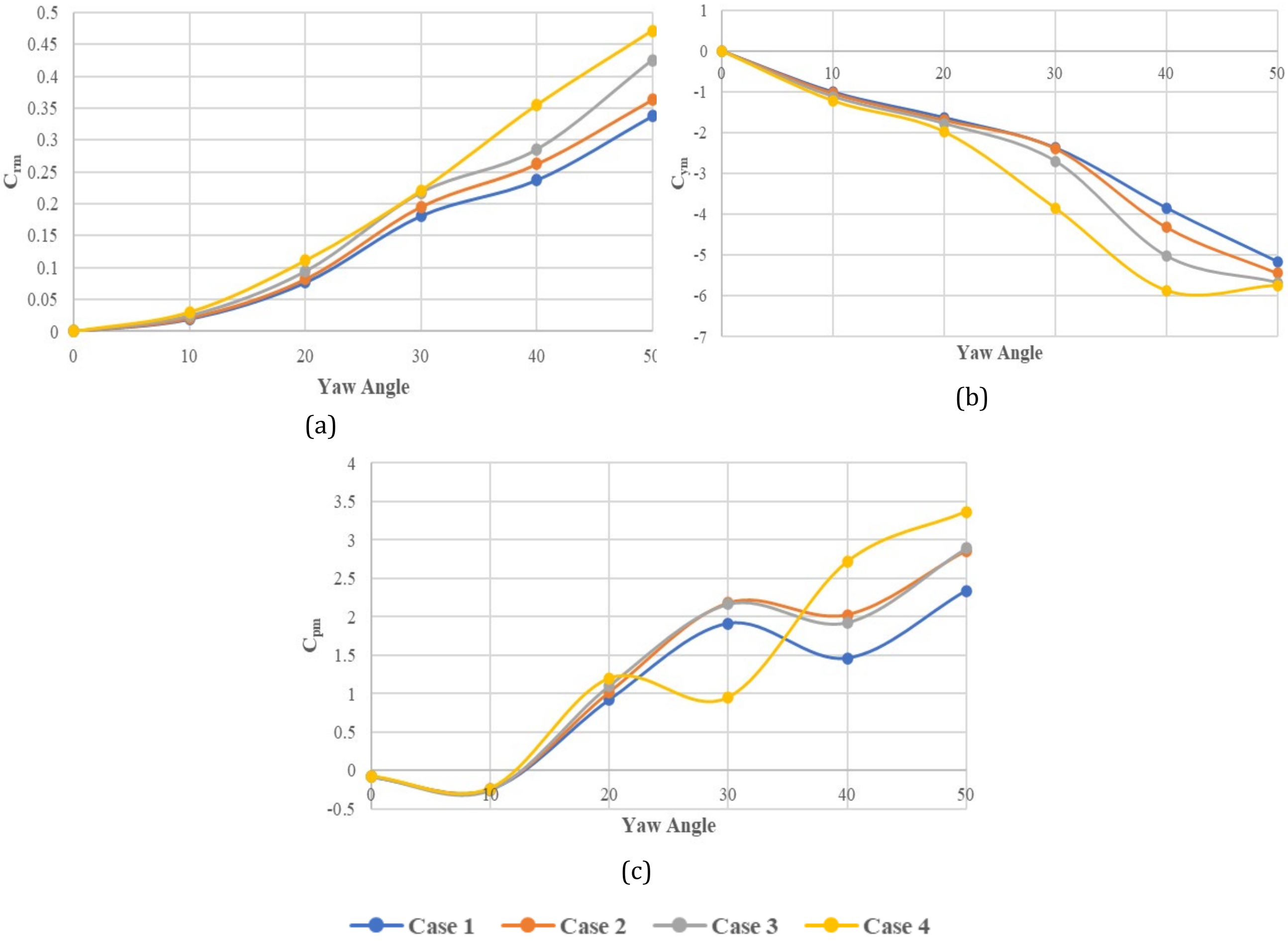

Fig. 11 *Time-averaged aerodynamic force and moment coefficients: (a) Rolling moment (C_{rm}); (b) Yawing moment (C_{ym}); (c) Pitching moment (C_{pm})*

4. Conclusion

The study's primary objectives, aimed to investigate the impact of varying embankment heights on the aerodynamic loads and the flow structure of a high-speed train under various crosswind conditions, are achieved successfully using computational fluid dynamics (CFD) analysis.

Initially, when the height of the embankment and crosswind yaw angles (ψ) are changed, aerodynamic loads change significantly. For instance, the side force coefficient (C_s) ranged from 0 to 15 for all the cases at ψ = 50. The train's rolling moment coefficients (C_{rm}) for various crosswind yaw angles and embankment heights. With rising embankment heights and yaw angles, the C_{rm} rises as well. From Ψ = 0° to Ψ = 30°, the C_{rm} value gradually increases in all four cases. Based on aerodynamic flow structure results, streamlines superimposed on pressure contour and vortex core shows that higher crosswind angles contribute to larger vortex formations. The formation of vortices becomes more complex and intense at higher yaw angles, which are 40° and 50°. As the height of the embankment increases, the crosswind is prevented from passing through the train, putting pressure on the train's surface and the windward side of the embankment. The intensity of vortex formation increases with crosswind angle and decreases toward the back of the train.

Acknowledgement

This research was financially supported by the Malaysia Ministry of Higher Education (MOHE) through Fundamental Research Grant Scheme (FRGS/1/2022/TK02/UTHM/03/1).

Conflict of Interest

Authors declare that there is no conflict of interest regarding the publication of the paper.

Author Contribution

The authors confirm their contribution to the paper as follows: ***study conception and design:*** *Nik Nur Amyra Adilla Noor Khairullah, Izuan Amin Ishak, Fadhilah Mohd Sakri;* ***data collection:*** *Nik Nur Amyra Adilla Noor Khairullah;* ***analysis and interpretation of results:*** *Nik Nur Amyra Adilla Noor Khairullah, Mohammad Arafat;* ***draft manuscript preparation:*** *Nik Nur Amyra Adilla Noor Khairullah, Izuan Amin Ishak, Nurshafinaz Mohd Maruai, Amir Khalid. All authors reviewed the results and approved the final version of the manuscript.*

References

[1] I. A. Ishak, “Safety Guideline for a Generic Train Travelling on Different Platform Scenarios under the Influence of Crosswind,” *Int. J. Adv. Trends Comput. Sci. Eng.*, vol. 9, no. 1.4, pp. 138–150, 2020, doi: 10.30534/ijatcse/2020/2191.42020.

[2] I. A. Ishak, M. S. Mat Ali, M. F. Mohd Yakub, and S. A. Z. Shaikh Salim, “Effect of crosswinds on aerodynamic characteristics around a generic train model,” *Int. J. Rail Transp.*, vol. 7, no. 1, pp. 23–54, Jan. 2019, doi: 10.1080/23248378.2018.1424573

[3] F. Dorigatti, M. Sterling, C. J. Baker, and A. D. Quinn, “Crosswind effects on the stability of a model passenger train-A comparison of static and moving experiments,” *J. Wind Eng. Ind. Aerodyn.*, vol. 138, pp. 36–51, Mar. 2015, doi: 10.1016/j.jweia.2014.11.009.

[4] C. Baker, H. Hemida, S. Iwnicki, G. Xie, and D. Ongaro, “Integration of crosswind forces into train dynamic modelling,” *Proc. Inst. Mech. Eng. Part F J. Rail Rapid Transit*, vol. 225, no. 2, pp. 154–164, 2011, doi: 10.1177/2041301710392476.

[5] M. Zakarka, Š. Skuodis, G. Šiupšinskas, and J. Bielskus, “Compressive strength and thermal properties of sand-bentonite mixture,” *Open Geosci.*, vol. 13, no. 1, pp. 988–998, 2021, doi: 10.1515/geo-2020-0289.

[6] C. Proppe and C. Wetzel, “A probabilistic approach for assessing the crosswind stability of ground vehicles,” *Veh. Syst. Dyn.*, vol. 48, no. SUPPL. 1, pp. 411–428, Dec. 2010, doi: 10.1080/00423114.2010.482158.

[7] Y. Han, C. S. Cai, Z. Chen, and Z. Tian, “Aerodynamic characteristics of road vehicles and bridges under cross winds,” *Most*.

[8] B. Diedrichs, M. Sima, A. Orellano, and H. Tengstrand, “Crosswind stability of a high-speed train on a high embankment,” *Proc. Inst. Mech. Eng. Part F J. Rail Rapid Transit*, vol. 221, no. 2, pp. 205–225, Mar. 2007, doi: 10.1243/0954409JRRT126.

[9] D. Zhou, H. Q. Tian, M. Thompson, and J. Sheridan, “Numerical and experimental investigations of the flow around a high-speed train on an embankment under sidewind conditions,” in *Lecture Notes in Applied and Computational Mechanics*, vol. 79, 2016, pp. 113–130. doi: 10.1007/978-3-319-20122-1_7.

[10] Izuan Amin Ishak *et al.*, “Numerical Analysis on the Crosswind Influence Around a Generic Train Moving on Different Bridge Configurations,” *J. Adv. Res. Fluid Mech. Therm. Sci.*, vol. 89, no. 2, pp. 76–98, Dec. 2021, doi: 10.37934/arfmts.89.2.7698.

[11] H. Y. Chen, J. L. Ma, X. G. Qin, and H. Y. Aziz, “Influence of Pile Cap Effect on Piled Embankment Supporting High-Speed Railway,” *Adv. Struct. Eng.*, vol. 16, no. 8, pp. 1447–1455, Aug. 2013, doi: 10.1260/1369-4332.16.8.1447.

[12] F. Cheli, R. Corradi, D. Rocchi, G. Tomasini, and E. Maestrini, “Wind tunnel tests on train scale models to investigate the effect of infrastructure scenario,” *J. Wind Eng. Ind. Aerodyn.*, vol. 98, no. 6–7, pp. 353–362, Jun. 2010, doi: 10.1016/j.jweia.2010.01.001.

[13] J. Winter, “Novel Rail Vehicle Concepts for a High Speed Train: The Next Generation Train,” in *Civil-Comp Proceedings*, 2012. doi: 10.4203/ccp.98.22.

[14] M. Arafat and I. A. Ishak, “CFD Analysis of the Flow around Simplified Next-Generation Train Subjected to Crosswinds at Low Yaw Angles,” *CFD Lett.*, vol. 14, no. 3, pp. 129–139, Apr. 2022, doi: 10.37934/cfdl.14.3.129139.

[15] C. Chang, T. Li, D. Qin, and J. Zhang, “On the Scale Size of the Aerodynamic Characteristics of a High-Speed Train,” *J. Appl. Fluid Mech.*, vol. 15, no. 1, pp. 209–220, 2022, doi: 10.47176/jafm.15.01.33041.

[16] M. Arafat, I. Amin Ishak, A. F. Mohammad, A. Khalid, M. N. Mohmad Jaát, and M. F. Yasak, “Effect of Reynolds number on the wake of a Next-Generation High-Speed Train using CFD analysis,” *CFD Lett.*, vol. 15, no. 1, pp. 76–87, Jan. 2023, doi: 10.37934/cfdl.15.1.7687.

[17] M. Arafat, I. A. Ishak, and A. F. Mohammad, “Influence of mesh refinement on the accuracy of numerical results for Next-Generation High Speed Train,” Muar, Unpublished, 2022. doi: 10.31219/osf.io/85jdh.

[18] T. Li, D. Qin, and J. Zhang, “Effect of RANS Turbulence Model on Aerodynamic Behavior of Trains in Crosswind,” *Chinese J. Mech. Eng. (English Ed.*, vol. 32, no. 1, Dec. 2019, doi: 10.1186/s10033-019-0402-2.

[19] P. Marsh, D. Ranmuthugala, I. Penesis, and G. Thomas, “Three-dimensional numerical simulations of straight-bladed vertical axis tidal turbines investigating power output, torque ripple and mounting forces,” *Renew. Energy*, vol. 83, pp. 67–77, 2015, doi: 10.1016/j.renene.2015.04.014.

[20] F. Cheli, F. Ripamonti, D. Rocchi, and G. Tomasini, “Aerodynamic behaviour investigation of the new EMUV250 train to cross wind,” *J. Wind Eng. Ind. Aerodyn.*, vol. 98, no. 4–5, pp. 189–201, Apr. 2010, doi: 10.1016/j.jweia.2009.10.015.

[21] I. A. Ishak, M. S. M. Alia, and S. A. Z. S. Salim, "Mesh size refining for a simulation of flow around a generic train model," *Wind Struct.*, vol. 24, no. 3, pp. 223–247, Mar. 2017, doi: 10.12989/was.2017.24.3.223.
[22] M. Lee, G. Park, C. Park, and C. Kim, "Improvement of Grid Independence Test for Computational Fluid Dynamics Model of Building Based on Grid Resolution," *Adv. Civ. Eng.*, vol. 2020, 2020, doi: 10.1155/2020/8827936.
[23] M. M. Fragner, K. A. Weinman, R. Deiterding, U. Fey, and C. Wagner, "Comparison of Industrial and Scientific CFD Approaches for predicting Cross Wind Stability of the NGT2 Model Train Geometry," *Int. J. Railw. Technol.*, vol. 4, no. 1, pp. 1–28, 2015, doi: 10.4203/ijrt.4.1.1.